

Epi-third and second harmonic generation microscopic imaging of abnormal enamel

Szu-Yu Chen,¹ Chin-Ying Stephen Hsu,² and Chi-Kuang Sun^{1,3*}

¹Graduate Institute of Photonics and Optoelectronics and Department of Electrical Engineering, National Taiwan University, Taipei, Taiwan, R. O. C. 10617

²Department of Preventive Dentistry, Faculty of Dentistry, National University of Singapore, Singapore 119074

³Research Center for Applied Sciences, Academia Sinica, Taipei, Taiwan, R. O. C. 115

*Corresponding author: sun@cc.ee.ntu.edu.tw

Abstract: Enamel covers the tooth crown and is responsible for protecting the inner tissues of the teeth. It is thus clinically important to diagnose the anomalies in tooth enamel structures in the early stage for prevention and treatment. In this article, we report the epi-harmonic-generation-microscopic study of various abnormal enamel from the nature surface of human teeth. With a 1230 nm light source and with an epi-collection scheme, an imaging depth greater than 300 μ m can be achieved. The contrast sources of THG and SHG in the abnormal enamel have been identified and verified by comparing the images from the sound enamel with those from white spot lesions, cracks, and the irradiated enamel. Besides the previously reported interprismatic space, THG is found to be contributed from cracks or the material inhomogeneities inside the enamel prisms; while SHG is attributed to the strain-induced breakage of the 6/m point group symmetry. Combined with the high 3D spatial resolution and no energy release during imaging, our study shows that the infrared-laser-based epi-harmonic generation microscopy can provide different contrasts to differentiate the abnormal enamel from sound enamel and could provide a valuable tool for *in vivo* monitoring of both morphological changes and strain status of hydroxyapatite crystals in the enamel without sectioning and staining.

©2008 Optical Society of America

OCIS codes: (170.3880) Medical and biological imaging; (190.4160) Multiharmonic generation; (170.1850) Dentistry; (190.1900) Diagnostic applications of nonlinear optics

References and links

1. R. W. Fearnhead, *Tooth enamel* (Florence, 1989).
2. Y. C. Chiang, B. S. Lee, Y. L. Wang, Y. A. Cheng, Y. L. Chen, J. S. Shiau, D. M. Wang, and C. P. Lin, "Microstructural changes of enamel, dentin-enamel junction, and dentin induced by irradiating outer enamel surfaces with CO₂ laser," *Lasers Med. Sci.* **23**, 41-48 (2008).
3. A. H. Meckel, W. S. Griebstein, and R. J. Neal, "Structure of mature human dental enamel as observed by electron microscopy," *Arch. Oral Biol.* **10**, 775-783 (1965).
4. H. N. Newman, and D. F. G. Poole, "Observations with scanning and transmission electron-microscopy on structure of human surface enamel," *Arch. Oral Biol.* **19**, 1135-& (1974).
5. R. J. Radlanski, H. Renz, U. Willersinn, C. A. Cordis, and H. Duschner, "Outline and arrangement of enamel rods in human deciduous and permanent enamel. 3D-reconstructions obtained from CLSM and SEM images based on serial ground sections," *Oral Sci.* **109**, 409-414 (2001).
6. M. K. Yamada, M. Uo, S. Ohkawa, T. Akasaka, and A. Watari, "Non-contact surface morphology analysis of CO₂ laser-irradiated teeth by scanning electron microscope and confocal laser scanning microscope," *Mater. Trans.* **45**, 1033-1040 (2004).
7. M. K. Yamada, and F. Watari, "Imaging and non-contact profile analysis of Nd:YAG laser-irradiated teeth by scanning electron microscopy and confocal laser scanning microscopy," *Dent. Mater.* **22**, 556-568 (2003).
8. T. F. Watson, A. Azzopardi, M. Etman, P. C. Cheng, and S. K. Sidhu, "Confocal and multi-photon microscopy of dental hard tissues and biomaterials," *Am. J. Dent.* **13**, 19D-24D, (2000).
9. C. J. Lin, and F. J. Kao, "Harmonic generation microscopy of dental sections,," in Conference on Lasers and Electro-Optics/Quantum Electronics and Laser Science Conference, Technical Digest (Optical Society of America, 2003), paper CMG6, <http://www.opticsinfobase.org/abstract.cfm?URI-CLEO-2003-CMG6>

10. F. J. Kao, "The use of optical parametric oscillator for harmonic generation and two-photon UV fluorescence microscopy," *Microsc. Res. Tech.* **64**, 175-181 (2004).
11. C. K. Sun, "Higher harmonic generation microscopy," *Adv. Biochem. Engin./Biotechnol.* **95**, 17-56 (2005).
12. M. H. Chen, W. L. Chen, Y. Sun, P. T. Fwu, and C. Y. Dong, "Multiphoton autofluorescence and second-harmonic generation imaging of the tooth," *J. Biome. Opt.* **12**, 064018 (2007).
13. R. Elbaum, E. Tai, A. I. Perets, D. Oron, D. Ziskind, Y. Silberberg, and H. D. Wagner, "Dentin micro-architecture using harmonic generation microscopy," *J. Dent.* **35**, 150-155 (2007).
14. C. L. Darling, G. D. Huynh, and D. Fried, "Light scattering properties of natural and artificially demineralized dental enamel at 1310 nm," *J. Biome. Opt.* **11**, 034023 (2006).
15. C. K. Sun, S. W. Chu, S. Y. Chen, T. H. Tsai, T. M. Liu, C. Y. Lin, and H. J. Tsai, "Higher harmonic generation microscopy for developmental biology," *J. Struct. Bio.* **147**, 19-30 (2004).
16. D. J. White, K. M. Kozak, J. R. Zoladz, H. J. Duschner, and H. Gotz, "Effects of Crest whitestrips bleaching on subsurface microhardness and ultrastructure of tooth enamel and coronal dentin," *Am. J. Dent.* **17**, 5-11 (2004).
17. Y. Barad, H. Eisenberg, M. Horowitz, and Y. Silberberg, "Nonlinear scanning laser microscopy by third harmonic generation," *Appl. Phys. Lett.* **70**, 922-924 (1996).
18. E. Sanchez-Pastenes, and J. Reyes-Gasga, "Determination of the point and space groups for hydroxyapatite by computer simulation of CBED electron diffraction patterns," *Revista Mexicana De Fisica* **51**, 525-529 (2005).
19. E. F. Bres, "Space-group determination of human tooth-enamel crystals," *Acta Cryst.* **B49**, 56-62 (1993).
20. R. W. Boyd, *Nonlinear Optics* (Academic Press, 1992).
21. T. Zhao, H. Lu, F. Chen, G. Yang, and Z. Chen, "Stress-induced enhancement of second-order nonlinear optical susceptibilities of barium titanate films," *J. Appl. Phys.* **87**, 7448-7451 (2000).
22. I. L. Lyubchanskii, N. N. Dadoenkova, M. I. Lyubchanskii, Th. Rasing, J. W. Jeong, and S. C. Shin, "Second-harmonic generation from realistic film-substrate interfaces: The effects of strain," *Appl. Phys. Lett.* **76**, 1848-1850 (2000).
23. C. Zhang, X. Xiao, N. Wang, K. K. Fung, and M. M. T. Loy, Z. Chen, and J. Zhou, "Defect-enhanced second-harmonic generation in (Si_mGe_n)_p superlattices," *Appl. Phys. Lett.* **72**, 2072-2074 (1998).
24. W. H. Jiang, and W. W. Cao, "Second harmonic generation of shear waves in crystals," *IEEE Trans. Ultrason. Ferroelectr. Freq. Control* **51**, 153-162 (2004).
25. T. T. Y. Huang, A. S. Jones, L. H. He, M. A. Darendeliler, and M. V. Swain, "Characterization of enamel white spot lesions using X-ray micro-tomography," *J. Dent.* **35**, 737-743 (2007).
26. Z. Amjad, P. G. Koutsoukos, and G. H. Nancollas, "The mineralization of enamel surfaces. A constant composition kinetics study," *J. Dent. Res.* **60**, 1783-1792 (1981).
27. T. E. Popowicz, J. M. rensberger, and S. W. Herring, "Enamel microstructure and microstrain in the fracture of human and pig molar cusps," *Arch. Oral Bio.* **49**, 595-605 (2004).
28. I. Ichim, Q. Li, W. Li, M. V. Swain, and J. Kieser, "Modelling of fracture behaviour in biomaterials," *Biomaterials* **28**, 1317-1326 (2007).
29. A. Wenzel, "Digital radiography and caries diagnosis," *Dentomaxillofacial Radiol.* **27**, 3-11 (1998).
30. M. O. Culjat, R. S. Singh, E. R. Brown, R. R. Neurgaonkar, D. C. Yoon, and S. N. White, "Ultrasound crack detection in a simulated human tooth," *Dentomaxillofacial Radiol.* **34**, 80-85 (2005).
31. A. Ribeiro, C. Rousseau, J. Girkin, A. Hall, R. Strang, C. J. Whitters, S. Creanor, and A. S. L. Gomes, "A preliminary technique for investigation of a spectroscopic the diagnosis of natural caries lesions," *J. Dent.* **33**, 73-78 (2005).
32. M. Fontana, Y. Li, A. J. dunipace, T. W. Noblitt, G. Fischer, B. P. Katz, and G. K. Stookey, "Measurement of enamel remineralization using microradiography and confocal microscopy-a correlational study," *Caries Research* **30**, 317-325 (1996).
33. A. Lussi, R. Hibst, and R. Paulus, "DIAGNOdent: an optical method for caries detection," *J. Dent. Res.* **83**, C80-C83 (2004).
34. E. D. J. Dejong, F. Sundstrom, H. Westerling, S. Transeus, J. J. Tenbosch, and B. Angmarmansson, "A new method for in-vivo quantification of changes in initial enamel caries with laser fluorescence," *Caries Res.* **29**, 2-7 (1995).
35. M. A. Pogrel, D. F. Muff, and G. W. Marshall, "Structural changes in dental enamel induced by high energy continuous wave carbon dioxide laser," *Lasers Surg. Med.* **13**, 89-96 (1993).
36. L. Aponte, and F. F. Feagin, "Effects of F- on recrystallization-remineralization and acid resistance of enamel," *J. Dent. Res.* **57**, 87 (1978).
37. B. O. Fowler, and S. Kuroda, "Changes in heated and in laser-irradiated human tooth enamel and their probable effects on solubility," *Calcif. Tissue Int.* **38**, 197-208 (1986).
38. H. C. Kim, K. S. Lee, O. S. Kweon, C. G. Aneziris, and I. J. Kim, "Crack healing, reopening and thermal expansion behavior of Al₂TiO₅ ceramics at high temperature," *J. Eur. Ceram. Soc.* **27**, 1431-1434 (2007).
39. L. D. Cynthia, and D. Fried, "Real-time near IR (1310nm) imaging of CO₂ laser ablation of enamel," *Opt. Express* **16**, 2685-2693 (2008).
40. C. P. Lin, F. H. Lin, Y. C. Tseng, S. H. Kok, W. H. Lan, and J. D. Liao, "Treatment of tooth fracture by medium energy CO₂ laser and DP-bioactive glass paste: compositional, structural and phase changes of DP-bioglass paste after irradiation by CO₂ laser," *Biomaterials* **21**, 637-643 (2000).

41. J. Serbin, T. Bauer, C. Fallnich, A. Kasenbacher, and W. H. Arnold, "Femtosecond laser as novel tool in dental surgery," *Appl. Surf. Sci.* **197**, 737-740 (2002).
 42. C. L. Tsai, Y. T. Lin, S. T. Huang, and H. W. Chang, "In vitro acid resistance of CO₂ and Nd-YAG laser treated human tooth enamel," *Caries Res.* **36**, 423-427 (2002).
-

1. Introduction

Teeth are made up of four different types of tissues. Among them, tooth enamel is the hardest and most highly mineralized tissue of the body. It covers the tooth crown and is responsible for protecting the inner tissues: dentin, cementum, and dental pulp, from mechanical, thermal, and chemical attack, as well as bacterial infection. Any developmental disorders or artifacts of enamel can let acid and bacteria penetrate into inner tissues and lead to dental diseases such as caries. It is thus clinically significant to diagnose the anomalies in tooth enamel structures in the early stage for prevention and treatment. According to previous researches, enamel is known to be 96% mineralized by weight and composed of a singular crystalline structure, hydroxyapatite (HA) crystal [1]. HA crystals are highly oriented and packed into rod-like structures, which are so-called enamel rods or prisms. The crystals are clustered together in prisms with diameters of 4 μ m, and each crystal is approximately 30 to 40nm in diameter and 10 μ m in length [2]. Not only the prism orientation but also the crystal arrangement within a prism is quite complex, and many techniques such as scanning transmission electron microscopy [3-5] and confocal laser scanning microscopy [5-7] have been used to investigate. Although much is known about the complex interrelationships of enamel prisms with undulating course, the frequently used thin enamel sections can only contain short segments of prisms and may not provide a complete picture of the prism orientation and interrelationship. Therefore, a high-penetration and high-spatial resolution technique is desired to provide the three-dimensional prism characterization, including the inhomogeneity of HA crystals and the strain inside the prism without sectioning and staining, ideal for least-invasive early enamel disease diagnosis.

Recently, two-photon fluorescence (TPF) microscopy and harmonic generation microscopy (HGM) have been used to investigate the dental structures, including enamel and dentine, from the processed surfaces of human teeth [8-13]. Although TPF, third-harmonic-generation (THG), and second-harmonic-generation (SHG) can all be found in dentine, no SHG was found in the tooth enamel [9,10,12], confirmed by a wavelength-dependent study [10]. In the tooth enamel, TPF based on a near infrared femtosecond excitation (700~900nm) can be used to reveal the morphological features of the enamel prisms. However, due to strong light scattering in the enamel within this range of excitation wavelength [14], the imaging depth was limited to several tens of microns [12]. According to a previous study with the ballistic transmission measurements, enamel has the highest transparency in the infrared (IR) region near 1310nm [14]. A previous study in a processed thin dental section based on an optical parametric oscillator with a 1270nm wavelength shows THG signals generated from the interprismatic spaces in a forward collection scheme [9]. It is thus highly desirable to move the excitation wavelength to this IR region for deeper penetration, while harmonic generation signals can provide the suitable nonlinear contrast for high sectioning capability.

In this study, we apply the 1230nm based harmonic generation microscopy for abnormal enamel imaging from the nature surface of intact human teeth with an epi-signal collection scheme for potential clinical application. With a 1230nm light source and with an epi-collection scheme, a HGM imaging with depth greater than 300 μ m is demonstrated in this study. The contrast sources of THG and SHG in the abnormal enamel have been identified and verified by comparing the images from the sound enamel, white spot lesions, cracks, and the artificially-lased enamel. Besides the previously reported interprismatic spaces, THG is found to be also contributed from the material inhomogeneities inside the enamel prisms or cracks; while the observed SHG is attributed to the strain-induced breakage of the 6/m point group symmetry. Combined with the high 3D spatial resolution and no energy release during HGM imaging, our study shows that the IR-laser-based epi-harmonic generation microscopy

could potentially be a valuable tool for in vivo monitoring of both morphological changes and strain status of hydroxyapatite crystals in the enamel without sectioning and staining.

2. Material and methods

The harmonic generation microscopic imaging of the tooth enamel was performed with a femtosecond Cr:forsterite laser centered at 1230nm with a 140fs pulse width at a 110MHz repetition rate. This experiment was performed with an IRB approval of the Review Committee of College of Medicine of National Taiwan University (NTUH-REC No.:200710020R). To investigate extracted tooth blocks through their natural tooth surfaces, an epi-collection geometry was used to collect higher harmonic signals and the setup schematic of the epi-HGM is shown in Fig. 1. The 1230nm IR laser beam was first shaped by a telescope and then directed into a modified beam scanning system (Olympus Fluoview 300). After passing through a pair of galvanometer mirrors and a microscope (Olympus BX-51), the scanning beam was focused on the natural enamel surface of an intact human tooth (Fig. 1(b)) by a water-immersion objective with NA of 0.9 (LUMplanFL/IR 60X/NA 0.9). Average illumination power of 100mW was applied to the sample surface during the observation. The excited SHG and THG signals were backward-collected by the same objective. Finally, the collected signals were divided into SHG (615nm) and THG (410nm) by a beamsplitter and then sent into two photomultipliers (PMT) with 410 and 615nm narrowband interference filters in front, separately. With computer processing, both SHG and THG images could be obtained and represented by green and yellow pseudo-colors, respectively. Moreover, 3D images could be reconstructed from a series of images obtained at different depths in the studied tooth enamel. With the IRB approval of the Institutional Review Board, National University of Singapore (NUS-IRB 04-154E), the CO₂ laser treatment was performed on the natural tooth surface of the extracted teeth.

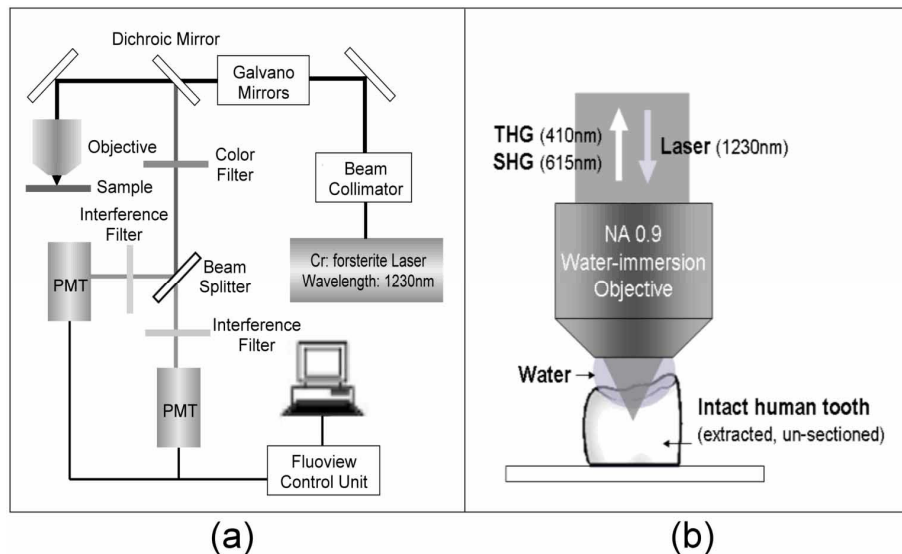


Fig. 1. Schematics showing (a) the experimental setup of the epi-harmonic generation microscope and (b) the detailed arrangement between the water-immersion objective and a studied intact human tooth, which was extracted but not sectioned.

3. Results and discussion

Different from the fluorescence-based techniques, harmonic generation, in which only virtual state transitions are involved, is known to obey the energy conservation rule and deposit no energy in interacted tissues [15]. Combined with an IR laser source, not only least-invasiveness can be achieved but also the penetration depth, measured from the natural

surface of the tooth, can be increased to several hundred microns in tooth enamel. In theory, THG is sensitive to interfaces with discontinuity of linear ($\chi^{(1)}$) and third-order nonlinear ($\chi^{(3)}$) susceptibility [15], and the greater the difference of $\chi^{(1)}$ or $\chi^{(3)}$ is, the stronger THG one can observe. Epi-THG should thus provide a contrast similar to that of the reflection-confocal microscopy [8,16], with an improved spatial resolution due to high nonlinearity. On the other hand, since SHG can only arise from non-centrosymmetric and highly-organized structures [17], the highly oriented HA crystalline in the tooth enamel may be considered as a possible source of SHG signals. However, a previous wavelength-dependent SHG study of sound enamel [10] clearly indicated that no SHG could be found either from inorganic crystals or the surrounding organic matrix. According to previous researches, despite a hexagonal symmetry, the HA crystal belongs to the 6/m point group [18,19], and it is well-known that all elements of the second-order susceptibility tensor ($\chi^{(2)}$) for the 6/m group vanishes [20]. We thus expect no SHG to arise from ideal HA crystals unless the crystal symmetry is distorted by external strain [21-24].

3.1 THG imaging of the sound tooth enamel from the natural tooth surface

Because of the large difference of $\chi^{(1)}$ and $\chi^{(3)}$ properties between the prisms and the thin (much less than the optical wavelength) organic-matrix-filled interprismatic space, THG was previously reported to provide contrast for the interprismatic spaces. As for SHG, no SHG was found in previous enamel studies. To serve as a comparison group to the HGM studies on the diseased enamel, we first performed epi-HGM imaging on sound tooth enamel. Following our experimental findings as shown in Fig. 2, similar to previous transmission type HGM experiments, no significant SHG was found in sound enamel while epi-THG generated from the interprismatic spaces successfully revealed the prism structure and distribution in the enamel. Different from the previous transmission study in a sectioned tooth sample with weak THG signals [9,10], our epi-THG study showed strong epi-THG signals which allowed us to image up to a penetration depth greater than 300 μm below the natural tooth surface. Figure 2 shows a series of epi-THG images (with no SHG detected) obtained from different depths, 10 μm , 60 μm , 120 μm , 180 μm , 240 μm , and 300 μm , beneath the natural tooth surface. The interprismatic spaces between prisms were found to be revealed by strong THG signals and the structures and distribution of the enamel prisms were depicted clearly. According to previous histological studies, the HA crystals are approximately 30 to 40nm in diameter and 10 μm in length, and the crystals are clustered together in prisms with a diameter around 4 μm [2]. It is also known that at the superficial layer, the prisms are more perpendicular to the tooth surface, but the direction of the prism becomes more parallel to the surface as going deeper into the enamel [1]. In the laterally-sectioned THG image of the superficial layer (Fig. 2(a)), the prisms were shown to be in a honeycomb structure, which indicated that the prisms were more perpendicular to the enamel surface. In Fig. 2(a), the planar prism-spacing was shown to be about 5 μm , indicating a declining angle around the order of 40 degrees, based on the previous histology result that the human enamel prisms are with an average of 4 μm in diameter. Deeper inside the enamel, from Fig. 2(b) to 2(f), the honeycomb-shaped lateral structure was found to be replaced by a strip-like lateral structure, indicating the direction of prisms turned to be more parallel to the enamel surface. Even at a depth of 300 μm , the prism structure could still be revealed through the 1230nm based epi-THG microscopy. In addition to lateral sections, the prism orientation of the enamel could also be revealed from the axially (XZ) sectioned epi-THG images. Figure 2(g) shows an axially sectioned epi-THG image with a total depth of 200 μm , confirming the above discussed declining angles. Due to the limited dynamic range in the displayed image and the attenuation of the THG signals in deeper layers, to make the weaker signals visible, the voltage of the PMT was adjusted to be higher to provide more gain starting at the depth of 100 μm . Without any sample preparation, our study indicated that the 3D prism orientation and interrelationship can be revealed by epi-THG imaging with the most natural condition preserved.

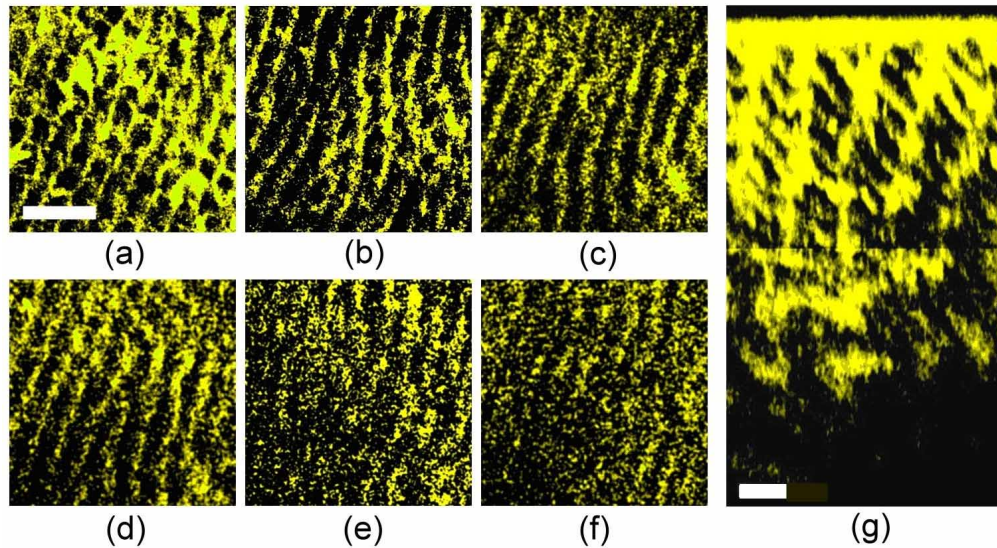


Fig. 2. Laterally-sectioned epi-THG images taken inside the enamel of an intact human tooth obtained at a depth of (a) 10 μm , (b) 60 μm , (c) 120 μm , (d) 180 μm , (e) 240 μm , and (f) 300 μm . (g) shows an axially-sectioned epi-THG image of the enamel, with a total depth of 200 μm and the prism orientation in the axial direction was successfully revealed. Due to the signal attenuation in deeper regions, the voltage of the PMT was adjusted at the depth of 100 μm . Epi-THG signals are represented by yellow pseudo-color. Scale bar: 20 μm .

3.2 SHG and THG imaging of white spot lesions in tooth enamel

As shown in Fig. 2 in sound dental enamel, due to the structure homogeneity of HA crystals inside the prisms, the dominant THG contrast comes from the organic-matrix-filled interprismatic space rather than the inorganic crystalline regions inside the prisms. For diseased enamel with HA crystal inhomogeneity we thus expect THG to be generated inside the prism to reflect the distinctive crystal abnormality. Similarly, although no SHG signals were expected and observed in the previous study of the sound enamel due to the 6/m point group symmetry of the HA crystals [20], this symmetry can possibly be broken to provide SHG signals if any strain exists [21-24]. It is thus highly desirable to study the THG and SHG signals inside the abnormal tooth enamel to evaluate the value of the HGM in noninvasive diagnosis of enamel diseases.

Different from sound tooth enamel, many kinds of chemical and morphological changes, such as white spot lesions and cracks, often take place in the enamel, especially in the superficial layer of the enamel. Among them, white spot lesion marks the beginning cavities and is mainly caused by mineral loss. In the region with white spot lesion, the chemical compositions of the HA crystal are different from the sound enamel due to demineralization and crystal inhomogeneity [25,26]. Thus, induced optical inhomogeneity within the prisms would provide the desired source of THG signals. Nevertheless, in the case of cracks, not only the THG from the cracks but also the SHG arising from the strains around the cracks are expected [27,28], due to the broken 6/m point group symmetry. To test our hypothesis, SHG and THG images were taken in areas with “natural” white spot lesions and cracks in the enamels of intact abnormal teeth. Figures 3(a)-(c) and 3(d)-(f) show example epi-HGM images obtained from the region with white spot lesions in a human tooth block beneath the natural tooth surfaces. The THG image contained some hollow structures (as shown in Fig. 2) but also some half-filled and completely filled prism structures, due to different degrees of mineral loss and subsequent optical inhomogeneity. Moreover, different from the case of sound enamel exhibiting no SHG signals, SHG could also be found in the region with white spot lesions (Figs. 3(b) and 3(e)).

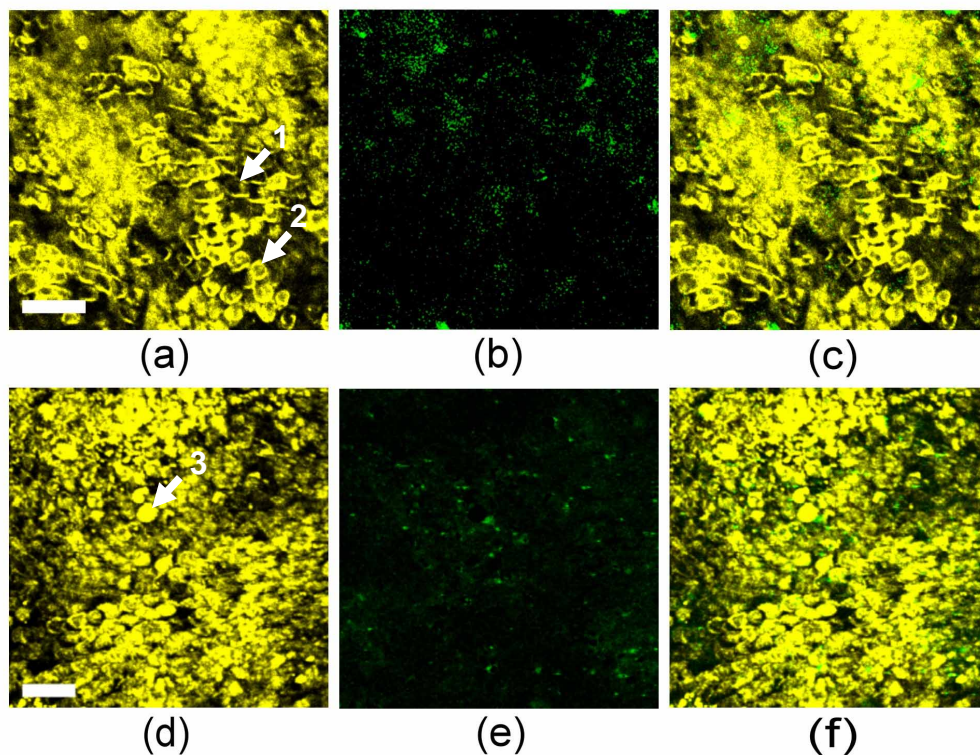


Fig. 3. (a) Epi-THG, (b) epi-SHG, and (c) combined images of the natural white spot lesion on a human tooth block beneath the natural tooth surface. THG signals generated inside prisms indicate the inhomogeneous arrangements of crystallites in the prisms. The THG image contained some hollow structures (arrow-1) but also some half-filled (arrow-2) and completely filled (arrow-3) prism structures, due to different degrees of mineral loss and subsequent optical inhomogeneity. (d), (e), and (f) shows the epi-THG, epi-SHG, and the combined images of another region with white spot lesion. THG and SHG signals are represented by yellow and green pseudo-colors, respectively. Scale bar: 50 μ m.

Figures 4(a) and 4(b) show example laterally-sectioned epi-THG and epi-SHG images, respectively, obtained from the region with natural cracks resulting from mechanical damages, and Fig. 4(c) shows the combined HGM image. In the tooth enamel, cracks mainly result from the mechanical and thermal stress, and the stress-strain exists around the cracks [27,28]. It is well known in previously studies that strain in crystals can cause the change in symmetry and thus induce SHG [21-24], including hexagonal symmetry crystals [24]. Therefore, the SHG arising from the cracks and surrounding prisms due to strains can be expected. In the THG image, both the crack and the enamel prisms beside the crack were clearly revealed, while SHG signals were also found at the sites of the cracks, with the breakage of the $6/m$ point group symmetry due to strain, agreeing well with our anticipation.

Tooth enamel is the outermost layer covering the tooth crown and protecting the inner tissues. Since many dental diseases take place at tooth enamel in their early phase, early diagnoses of enamel abnormalities may have clinical significance. Various tools have been developed for enamel diagnosis, such as radiography [29], ultrasound detection [30], spectroscopy [31], confocal microscopy [32], and DIAGNOdent [33] etc. Radiography and ultrasound detection can be used to image the cracks on the tooth enamel. Based on the autofluorescence emitted from caries [34], spectroscopy and confocal microscopy can help to detect caries. However, some limitations such as poor spatial resolution and invasive nature have limited their precision and possible applications. Therefore, a noninvasive diagnostic tool with high spatial resolution is desired. With THG sensitive to the inhomogeneity among

the prisms and SHG sensitive to the strains status in abnormal enamel, the results of our study have demonstrated the feasibility to use the 1230nm based epi-HGM for early detection of enamel lesions, advantaged with the non-invasive nature, high spatial resolution, and high penetration capability of the HGM system.

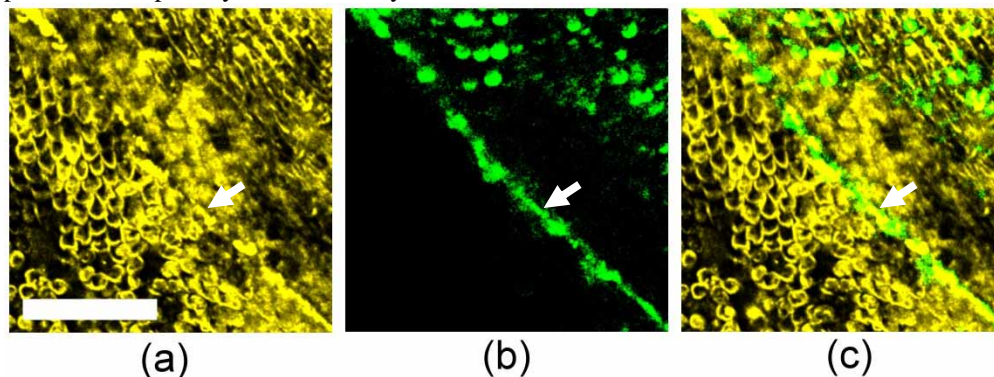


Fig. 4. (a) Epi-THG and (b) epi-SHG images of the crack in a human tooth block beneath the natural tooth surface. THG signals revealed both the crack and the enamel prisms beside, while SHG revealed the strain status around the crack (arrows). (c) Combined image. THG and SHG signals are represented by yellow and green pseudo-colors, respectively. Scale bar: 50 μ m.

3.3 SHG and THG imaging of lased tooth enamel

For further experimental verification on the source of the harmonic generation signals, we performed the SHG and THG imaging on irradiated human tooth enamel. According to the previous studies using CO₂ lasers to irradiate the enamel surface, different morphological and micro-structural changes could be found at different depths beneath the lased enamel surface depending on the temperature distribution [35-37]. Since tooth enamel is composed of both organic and inorganic materials and the thermal expansion coefficients of these materials are different, heat-induced cracks due to thermal expansion would take place, and strains will be generated around the cracks [38]. Based on the discussion above, THG and SHG would both be expected to appear around the heat-induced cracks. At the superficial layer irradiated with the highest energy level and the high induced temperature, both melting and heat-induced cracks appeared. As the deeper layer absorbed less energy, with lower induced temperature, the heat-resulted melting will become less and cause less cracks and strains. Therefore, different morphological changes and strain status are expected to be found, reflected by the HGM signals.

Figures 5(a), 5(b) and 5(c) show respectively the epi-THG, epi-SHG, and the combined images of the tooth enamel obtained at a depth of 10 μ m beneath the lased surface. The tooth was irradiated by a CO₂ laser (10.6 μ m) with a pulse energy of 100mJ and a repetition rate of 2Hz for a period of 5sec. During the irradiation, no water cooling was applied. In Fig. 5(a), the interface-sensitive THG revealed the heat-induced cracks while in Fig. 5(b) the strain at the cracks is nicely presented with SHG signals. Due to melting at this superficial layer, the corresponding THG signals from the interprismatic space were found to be significantly reduced, agreeing with our anticipations. Strong THG and SHG signals can be observed around the heat-induced cracks. Figures 5(d), 5(e), and 5(f) show respectively the epi-THG, epi-SHG, and the combined images taken at a deeper depth of 55 μ m beneath the same lased surface. Due to the reduced absorption energy at this depth and the weaker prism melting effect, strain-sensitive SHG signal was found to become weaker as expected, while THG signals generated from the interprismatic spaces were found to be recovered. By controlling the PMT voltages at these two depths to be the same 1000V and by comparing the signal intensities of the THG images, the much decreased SHG signal in the deeper layer (Fig. 5(e)) can not be attributed to the signal degradation due to the penetration capability of our system. Based on the THG and the corresponding SHG images, this control study supports our

previous hypothesis that the SHG signals reflect the strain distribution, which locates around the heat-induced cracks and decreases with depth [39,40].

Recently, laser therapy studies have demonstrated many promising dental applications. For example, short pulse lasers with a medium energy have been applied for dental surgery [41]. Nd-YAG laser has been used to increase the acid resistance of tooth enamel or applied to caries removal [42], and CO₂ laser treatment was used to bridge the tooth fractures [40]. However, noninvasive morphological and functional characterization of enamel is critical in identification of the optimal operational parameters to minimize the potential laser-induced thermal/mechanical side effects. Compared with the invasive SEM characterization, our study has confirmed that epi-HGM may be a promising tool to provide *in vivo* structural and strain information to facilitate the clinical/dental application of these innovative laser therapies.

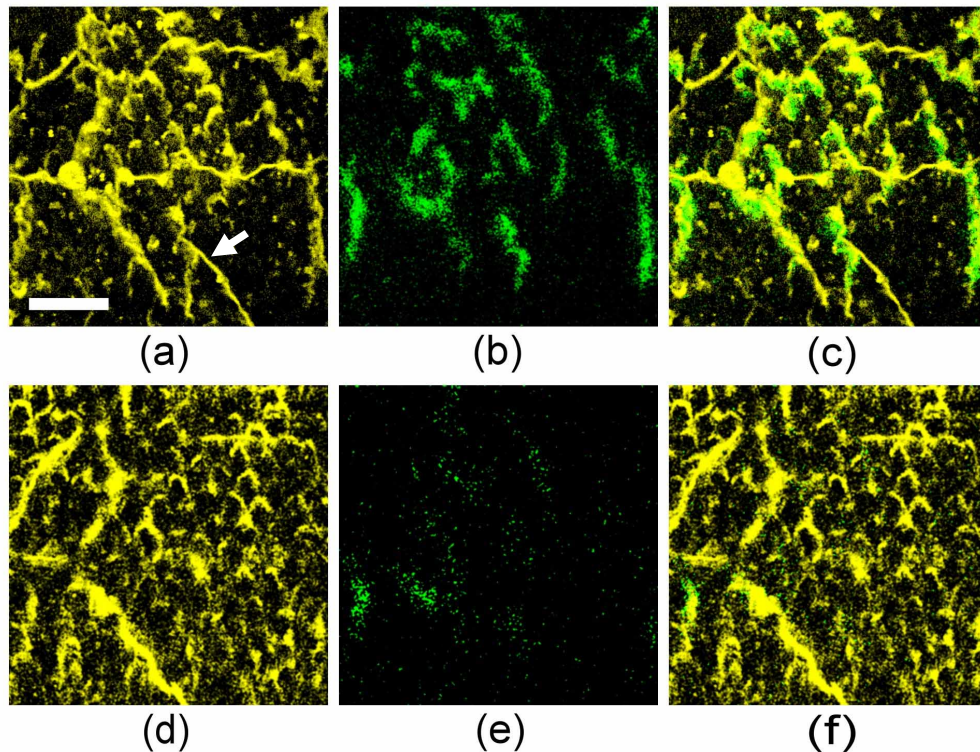


Fig. 5. The laterally sectioned (a) epi-THG and (b) epi-SHG images of a lased human tooth block taken at a depth of 10 μ m beneath the lased enamel surface, and (c) is the combined image. (d) and (e) show the laterally-sectioned epi-THG and epi-SHG images obtained at a depth of 55 μ m beneath the same lased surface, and (f) is the combined image. In the epi-THG images, both the heat-induced cracks (arrow) and the prism structures were observed, while the strong SHG signals arising from the heat-induced cracks indicate the strained status around the cracks. Epi-THG and epi-SHG images are represented by yellow and green pseudo-colors, respectively. Scale bar: 20 μ m.

4. Conclusion

In this article, we report the harmonic generation microscopic study of tooth enamel with a 1230nm light source. In an intact human tooth and with an epi-collection scheme, an imaging depth greater than 300 μ m was achieved. The contrast sources of THG and SHG in the enamel have been identified and verified by comparing the images from the sound tooth enamel, white spot lesions, cracks, and the irradiated tooth enamel. THG signals are contributed from the material inhomogeneity inside and between the enamel prisms as well as cracks. SHG signals are contributed from the strain-induced breakage of the 6/m point group symmetry.

From THG images, the crystal inhomogeneity in white spot lesions and morphological changes at cracks can be revealed, while the strains at the cracks can be shown by the strain-sensitive SHG. Furthermore, the well-known micro-structural changes induced by CO₂ laser irradiation was also used to further verify the proposed contrast origins. From the HGM images obtained at different depths beneath the lased surface, the different morphological changes and strain status under different energy levels were observed by structure-sensitive THG and strain-sensitive SHG respectively. Our study shows that the infrared-laser-based epi-harmonic generation microscopy can provide different contrasts to differentiate the abnormal enamel from sound enamel with a high spatial resolution could be a valuable tool for *in vivo* monitoring both the morphological changes and strain status of HA crystals in the tooth enamel without sectioning or staining. This research is sponsored by National Health Research Institute of Taiwan (NHRI-EX97-9201ED), National Taiwan University Research Center for Medical Excellence, The Frontier Research Grant of NTU (95R0110), and by A* Star Biomedical Research Council (BMRC grant 222-000-015-305), Singapore.